Journal of Power Sources 196 (2011) 8897–8903

Contents lists available at ScienceDirect

Journal of Power Sources

journal homepage: www.elsevier.com/locate/jpowsour

Improvement on the long-term stability of flexible plastic dye-sensitized solar cells

Kun-Mu Lee[a,*], Wei-Hao Chiu[b], Ming-De Lu[a], Wen-Feng Hsieh[b,c,**]

[a] Green Energy & Environment Research Laboratories, Industrial Technology Research Institute, Hsinchu 31040, Taiwan
[b] Department of Photonics & Institute of Electro-Optical Engineering, National Chiao Tung University, 1001 Tahsueh Road, Hsinchu 30050, Taiwan
[c] Department of Photonics & Institute of Electro-Optical Science and Engineering, National Cheng Kung University,1 University Road, Tainan 701, Taiwan

ARTICLE INFO

Article history:
Received 28 January 2011
Received in revised form 6 May 2011
Accepted 15 June 2011
Available online 22 June 2011

Key words:
Plastic dye-sensitized solar cell
Long-term stability
Organic iodide
Flexible

ABSTRACT

We investigate the long-term stability of performance for plastic dye-sensitized solar cells (DSSCs) based on organic iodides (TBAI or PMII) in methoxypropionitrile-based electrolytes. Plastic DSSCs containing TBAI maintain 96.9% of baseline efficiency under more than 1000 h prolonged one sun light irradiation and thermal stress (60 °C) aging. The factors of device long-term stability, such as the effects of organic iodides, cell-sealing conditions, and the sheet resistance of indium tin oxide coated polyethylene naphthalate substrate (ITO/PEN) are discussed via using electrochemical impedance spectroscopy and electrical resistance measurement.

1. Introduction

Researchers have studied the photovoltaic applications of dye-sensitized solar cells (DSSCs) due to their high conversion efficiency and low cost [1]. A DSSC generates photocurrent through ultra-fast injection of electrons from photo-excited dye molecules into the conduction band of a semiconductor such as TiO_2 or ZnO. This process is followed by dye regeneration and hole transportation to the counter electrode. Currently, one of DSSC research has been focused on the development of flexible plastic substrates. The low-temperature (<150 °C) treatment of semiconductor materials is a crucial technology in the manufacture of plastic DSSCs due to the low melting points of the substrates. Several low-temperature techniques have been developed to address this issue, including chemical sintering [2], hydrothermal necking [3,4], microwave sintering [5,6], electrophoretic deposition (EPD) [7], and mechanical compressing [8–11]. Recently, we have made a high quality TiO_2 electrode by a multiple EPD process with binder-free TiO_2 nanoparticles (NPs) solution and applied it to a plastic DSSC with the conversion efficiency of ca. 6.6% at an illumination of 100 mW cm^{-2} [12].

For commercial applications, a DSSC must pass durability test in accelerated conditions such as 60–80 °C for 1000 h and exposure to continuous solar irradiation of 100 mW cm^{-2}. In many cases, the durability of DSSC is related to the leakage and deterioration of the electrolyte due to imperfections in the sealing material and process [13]. Several DSSC designs have been made to replace organic liquid electrolyte with gel electrolytes or solid-state electrolytes [14–17]. However, liquid electrolytes with solvents having high boiling temperature are still a better solution for DSSCs with mesoporous TiO_2 electrodes. Researchers are currently investigating the long-term stability of small cells and large-area DSSC modules under simulated solar light. These designs show good long-term stability under continuous irradiation of more than 1000 h, especially in the absence of UV light [18–22]. However, only few studies reported flexible DSSCs [13,23]. Therefore, in this study we develop a fabrication method of TiO_2 electrode at room temperature (RT) combining the EPD and compress processes for plastic DSSCs. We also investigate the effects of ITO properties and different iodides on photovoltaic performance and long-term stability. Finally, we report electrochemical impedance spectroscopy (EIS) analysis of variations in the electron transport resistance of the TiO_2 electrode (R_w), charge-transfer resistance related to electron combination (R_k), effective electron lifetime (τ_{eff}), electron diffusion coefficient (D_{eff}) and electron diffusion length (L_n) of devices during light-irradiation and thermal aging processes.

* Corresponding author. Tel.: +886 3 5913135; fax: +886 3 5834389.
** Corresponding author. Tel.: +886 3 5712121x56316; fax: +886 3 5716631.
E-mail addresses: kunmulee@itri.org.tw (K.-M. Lee), wfhsieh@mail.nctu.edu.tw (W.-F. Hsieh).

0378-7753/$ – see front matter © 2011 Elsevier B.V. All rights reserved.
doi:10.1016/j.jpowsour.2011.06.049

2. Experimental

Indium tin oxide (ITO)-coated polyethylene naphthalate (PEN) substrates (10 ohm sq^{-1}, thickness 120 μm, Tobe Inc., Japan) were cleaned with mild soap and ethanol, thoroughly rinsed with deionized water (>18.2 MΩ), and then dried by a clean air stream. The mesoporous TiO_2 films were prepared by EPD. The TiO_2 suspension for electrophoretic deposition (EPD) consisted of 0.25 g P-90 TiO_2 NPs (a kind gift from Degussa AG, Germany) in 100 mL isopropyl alcohol (IPA) was stirred with a magnetic stirrer overnight and ultrasonically dispersed for 1.5 h before putting in the electrophoretic cell. The two electrophoretic electrodes of fluorine-doped tine oxide (F:SnO_2, FTO) conductive glass and ITO/PEN film were separated by 1.5 cm to serve as the cathode and anode, respectively.

A Kethley 2400 Source Meter served as a power supply for EPD providing different currents and deposition durations in constant current mode, which is more effective and controllable than constant voltage mode [24]. Fig. 1 presents sketch plots of the electrophoretic cell, the preparation of TiO_2 electrodes, and the parameters used in this process. In addition, a scattered layer made of TiO_2 NPs (approximately 100 nm in diameter, denoted by 100 nm TiO_2) was introduced on top of the light-absorbing layer. The optically scattering 100 nm TiO_2 NPs were synthesized in a basic solution using the sol–gel method. A colloidal suspension was made by mixing 58.6 g titanium isopropoxide with 290 mL distilled water. The mixture was then filtered and placed in an autoclave containing 20 mL tetramethylammonium hydroxide (TMAH) at 250 °C for 12 h. Finally, the solution in the autoclave was washed by DI water and centrifuged to obtain the 100 nm TiO_2 powder. After drying TiO_2-deposited ITO/PEN substrate at RT and one atmospheric pressure, a pressure treatment was applied to improve the adhesion of TiO_2 on the substrate and to enhance the photovoltaic performance of the device.

The mesoporous TiO_2 film was immersed in a solution of 0.5 mM N719 dye (cis-bis(isothiocyanato)bis(2,2′-bipyridyl-4,4′-dicarboxylato)-ruthenium(II) bis-tetrabutylammonium, Solaronix, Aubonne, Switzerland) in acetonitrile (AN, HPLC grade, J.T. Baker)/tert-butyl alcohol (t-BuOH) (v/v = 1/1) binary solvent at 40 °C for 4 h to absorb sufficient N719 dye for light harvesting. The dye-sensitized TiO_2 electrode was then rinsed with AN to remove the remaining dye, and dried under standard atmosphere conditions at RT. A platinum-sputtered ITO/PEN film served as the counter electrode. A two-electrode sandwich cell was separated by a 60 μm hot-melt type spacer and filled with the electrolyte. The effective working area of the device was limited to approximately 0.28 cm^2 by using a black mask.

The electrolyte used for the high conversion efficiency test consisted of 0.4 M LiI (Merck), 0.4 M tetrabutylammonium iodide (TBAI, Aldrich), 0.04 M I_2 and 0.5 M N-methylbenzimidazole (NMBI, Aldrich) in AN/methoxypropionitrile (MPN Alfa Aesar) mixture (v/v = 1/1). Low-volatility electrolytes with a composition of 0.8 M TBAI, 0.1 M I_2 (99.8%), and 0.5 M NMBI in MPN (electrolyte A) or 0.8 M 1-methyl 3-propyl imidazolium iodide (PMII), 0.1 M I_2, and 0.5 M NMBI in MPN (electrolyte B) were used to test the durability of plastic DSSCs. The above-mentioned chemicals were used as received without further purification.

The durability test in this study including 100 mW cm^{-2} light irradiation with the range from UV to IR and thermal stress (60 °C) aging of hermetically sealed cells was performed with a sun test xenon arc lamp (ATLAS Ci3000 xenon Fadeometer). Following a period of continuous light irradiation, photoelectrochemical measurements were taken after the cells cooled to RT. An UV-cut filter was commonly put onto DSSC to avoid the degradation of dye, but was not used in DSSC with PEN polymer substrates due to the cut-off incident light of about 380 nm by PEN substrates.

To measure current–voltage characteristics and electrochemical impedance spectroscopy (EIS), a white light source (Yamashita Denso, YSS-100A) provides an irradiance of 100 mW cm^{-2} (AM 1.5G) on the surface of the solar cell. EIS measurements were performed with a computer-controlled electrochemical analyzer (Autolab, PGSTAT30) at a temperature of 25 ± 2 °C. The forward bias set for the open circuit voltage (V_{OC}) with an AC amplitude of 10 mV was applied between the photoanode and counter electrode under the explored frequency ranging from 50 mHz to 1 MHz.

3. Results and discussion

The cross-section SEM images of the three kinds of EPD TiO_2 films are showed in Fig. 2a that are composed of TiO_2 crystalloid particles with a porous structure. The P-90 NPs size is about 15 nm and the optically scattering TiO_2 NPs is about 100 nm (also denoted by 100 nm TiO_2). The 100 nm TiO_2 was well-deposited on the transparent film composed by P-90 NPs without any lager pin holes and these three kinds of TiO_2 films were prepared to device assembling. Fig. 2b shows the typical monochromatic incident photon-to-electron conversion efficiency (IPCE) spectra, which is to scale the spectral response of the photovoltaic devices. Around the distinct peak at 540 nm attributed to the metal-to-ligand charge transfer absorption band of the N719 dye, the DSSCs with only P-90 NPs were obtained the IPCE value about 54% which was greater than the ones with only 100 nm NPs (IPCE value about 47%) because of the greater amount of the N719 dye on TiO_2 film. The DSSCs consisting of both P-90 and 100 nm NPs showed the greatest IPCE value of 60% due to enough surface area for dye absorption with good light scattering. The inset figure in Fig. 2b presented the normalized IPCE of three kinds of DSSCs. The shapes of the three IPCE curves are almost the same in the wavelength range of 400–600 nm On the other hands, in the wavelength range above 600 nm, the IPCE curves shapes with DSSCs consisting of 100 nm TiO_2 NPs were greater than the P-90 one, meaning of the lack of the light-scattering effect for P-90 NPs. It suggests that the high IPCE in DSSCs based on relatively thin films can be improved by enhanced light absorption with enough surface area for dye absorption and good light scattering layer with larger size NPs, which was consistent with the work reported by Arakawa et al. in 2004 [25]. On the other hand, a good quality film with no crack is necessary for electron collection that may also lead to an improvement in IPCE (Table 1).

Although the press treatment has been used on flexible substrate DSSCs [8–11], the correlation between applied pressure and device performance should also be clarified in this work. Therefore, a detailed experimental was performed under different compress pressure conditions to obtain the performance of the assembled DSSCs devices, and the results are shown in Fig. 3a. The thickness of electrophoretic deposited TiO_2 film is about 20 μm, and reduces to 6–8 μm via different applied pressures. Between a non-pressed and a 100 MPa-pressed TiO_2 films, J_{SC} increased rapidly from 1.7 to 11 mA cm^{-2}, respectively. When the external pressure applied on TiO_2 films is from 100 to 500 MPa, J_{SC} became a constant. It is believed that the high external pressure (over 100 MPa) not only melt the surface of TiO_2 NPs to form a good porous photoanode for electron transporting, but also increase the adhesion strength between the TiO_2 film and ITO/PEN substrate [26]. The slight changes of V_{OC} with different pressure from non-pressed to 400 MPa were not significant but related to the film thickness. The fill factor (FF) was observed almost a constant about 0.7 in the range 0 (non-pressed) to 400 MPa, but FF of the DSSCs with 500 MPa pressure dropped to 0.4 due to the occurring of crack in the ITO film. Consequently, the 6% overall conversion efficiency with 100 MPa pressure treatment was achieved. Fig. 3b shows the relationship between the time of the pressure applied for pressing the TiO_2 film

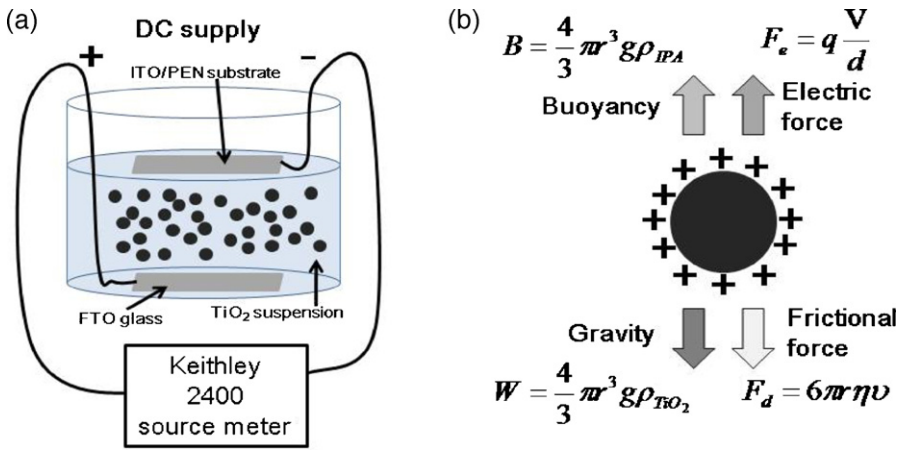

Fig. 1. Sketch plots of the electrophoretic cell, the preparation of TiO_2 electrodes, and the significant parameters in this process.

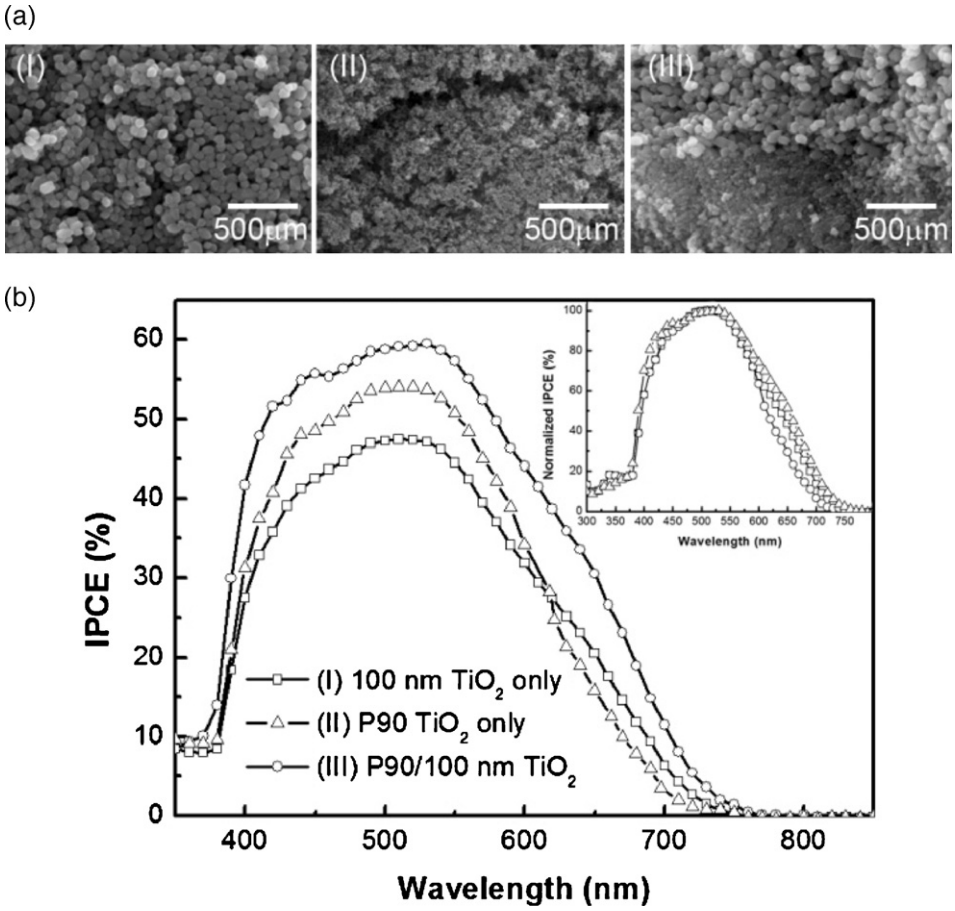

Fig. 2. (a) Cross-section SEM image of an EPD film for (I) 100 nm TiO_2; (II) P-90 TiO_2 and (III) P-90 TiO_2 and 100 nm TiO_2 as double-layer film on ITO/PEN substrate. (b) IPCE spectra and normalized IPCE spectra (inset figure) of DSSCs with these three kinds of nanocrystalline TiO_2 film.

Table 1
Physic-chemical property of TiO_2 particles used in this study.

Material	Specific surface area (BET) ($m^2\ g^{-1}$)	Average primary particle size (nm)	Crystal phase
P-90 TiO_2	90 ± 20	ca. 14	Anatase
100 nm TiO_2	30 ± 10	ca. 100	Anatase >99%

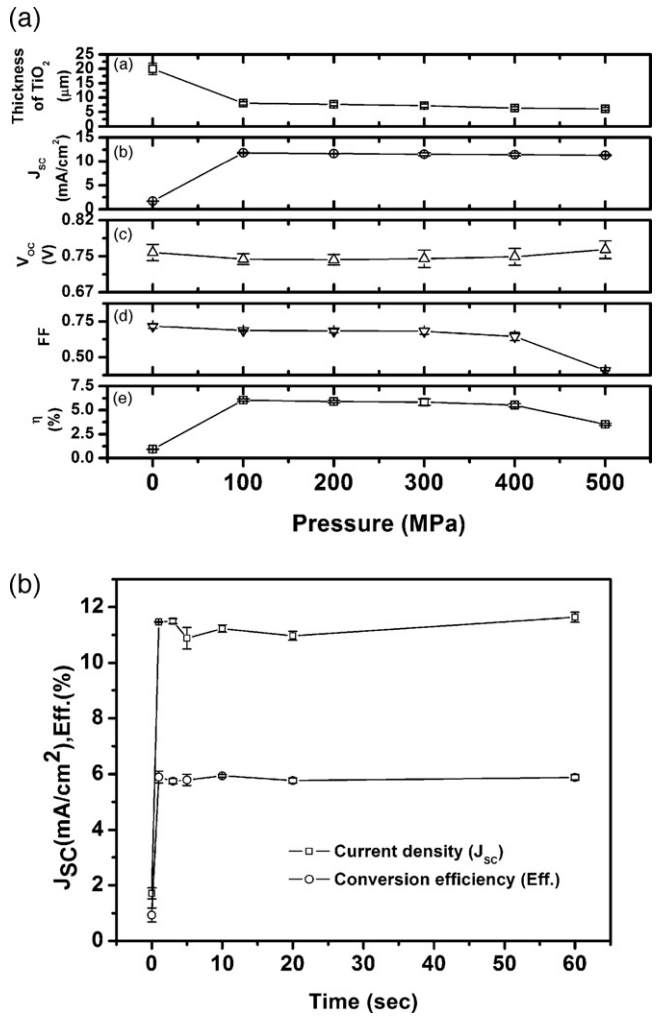

Fig. 3. (a) The correlation between the compression pressure of the electrophoretic deposited TiO_2 thin film and device performance. The parameters of the non-pressure photoanode were plotted at the 0 MPa position. (b) The correlation between the compression time of the electrophoretic deposited TiO_2 thin film and the current density and conversion efficiency, respectively.

and the performance of the assembled DSSCs. After the 100 MPa compressing, the thickness of the TiO_2 photoanodes used for this measurement were 7–8 μm. J_{SC} and the conversion efficiency were observed to be low in the absence of pressure treatment (0 s), and to be almost constant for a rapid pressure treatment (1 s) to a continued pressure treatment (60 s). It is suggested that the electron transporting in the photoanode and the adhesion strength between the TiO_2 film and ITO/PEN substrate can be significantly improved in a rapid time. As the results, it opens up the possibility of developing a continuous roll to roll process for mass production of flexible DSSCs.

Before investigating the durability of plastic DSSC, it is important to test the stability of ITO/PEN in electrolyte and to check the sealing material and condition in the plastic cell. Fig. 3a shows the variation of sheet resistance of ITO/PEN immersed in two electrolytes for 1000 h which are electrolyte I (0.5 M PMII/0.05 M I_2 in MPN) and electrolyte II (0.5 M LiI/0.05 M I_2 in MPN). The sheet resistance of ITO/PEN immersed in electrolyte I increases slightly from 11.2 to 12.2 ohm sq^{-1}; however, that in electrolyte II increases significantly from 11.1 to 18.6 ohm sq^{-1}. The OM images of ITO/PEN surface are also showed in Fig. 3b, which clearly observed by cracking phenomenon of ITO film after immersing in electrolyte II for 1000 h. This indicates that the ITO/PEN film in the electrolyte containing LiI is unstable, implying a chemical etching reaction [13].

A 60 μm hot-melt type spacer was used to seal the test cell for preventing the electrolyte from leaking. After heat-sealing at 125 °C for 10 s, the electrolyte consisted of 0.8 M PMII/0.1 M I_2/0.5 M NMBI in MPN was injected in the spacer between two electrodes through the injection holes. The injection holes and edge of the test cell were then sealed with a UV glue and cured under UV light for 15 s. Fig. 4 presents the test cell structure (inset image) and the weight loss data. The weight loss was only −0.43% after more than 2700 h at 60 °C in dark, indicating that the sealing condition was sufficient to avoid electrolyte leakage in plastic DSSCs.

For light aging test, the performance of the devices was tested under continuous light irradiation (100 mW cm^{-2}) at 60 °C. It increases to a maximum initially then maintains at a steady state after 100 h as shown in Fig. 5. The apparent increase in J_{SC} and conversion efficiency may be due to improvement in electrolyte penetration into the mesoporous TiO_2 film, lowering of the TiO_2 conduction band boundary and activation of the Pt-coated counter electrode as reported previously [27]. Note that devices exhibit different conversion efficiency improvements with different cation iodides. In Fig. 5a and b, J_{SC} and conversion efficiency of the device with electrolyte I increased significantly from 3.81 to 6.89 mA cm^{-2} and from 1.85% to 3.14%, respectively, under 100 h continuous light irradiation. On the other hand, the device with electrolyte II achieves an efficiency value of 2.38% from the initial value of 1.84%, which J_{SC} only slightly increases from 4.03 to 4.81 mA cm^{-2} in Fig. 5b. This improvement results from TBA^+ on the TiO_2 film surface that protected the voids in the dye-coated TiO_2 film in turn blocked undesirable interfacial charge recombination and suppressed surface protonation. The gradual decrease in conversion efficiency of cell after 100 h in Fig. 5b suggests that the conformation, dye alignment, and intermolecular interactions of N719 on the surface of TiO_2 film should change during the aging process.

To fairly evaluate device durability, the photovoltaic parameters of the devices at the steady state obtained after 100 h aging were used as a baseline. After continuous aging for 1000 h, the devices with electrolytes I and II still maintained 96.9% and 72.3% of the baseline efficiency measured at 100 h. This performance is better than that of previously reported [13,23]. The major factor of degradation in the efficiency of the devices is due to a decrease of V_{oc} (∼0.13 V) (see Fig. 5c) that is caused by surface protonation under the accelerated aging test [28–30].

To understand the effects of different cation iodides, TBAI and PMII, on charge transportation and device durability, the electrochemical impedance spectra (EIS) of the devices aged for 100, 500, and 1000 h were measured under open-circuit condition and illumination of 100 mW cm^{-2}. Fig. 6a–c shows the Nyquist plots of the impedance data, and the equivalent circuit model of DSSC is showed in Fig. 6d [31]. The TiO_2 working electrodes are characterized by the chemical capacitance $C\mu$, the transport resistance R_w and the TiO_2/electrolyte interfacial charge-transfer resistance R_k. The terms R_s and Z_N represent the charge transport resistance of ITO (including external circuit) and the finite Warburg impedance in the electrolyte. R_{Pt} and C_{Pt} represent the charge-transfer resistance and capacitance at the Pt surface; R_{ITO} and C_{ITO} represent the charge-transfer resistance and the interfacial capacitance at the ITO/electrolyte interface; finally, R_F and C_F represent the resistance and the capacitance at the ITO/TiO_2 interface.

The EIS-fitting data from these devices are listed in Table 2. The R_w values increase with light soaking time for electrolyte containing either TBAI or PMII that lowers the estimated electron diffusion coefficient (D_{eff}) and shortens the diffusion length, $L_n = L(R_k/R_w)^{1/2}$, where L is the thickness of TiO_2 film. However,

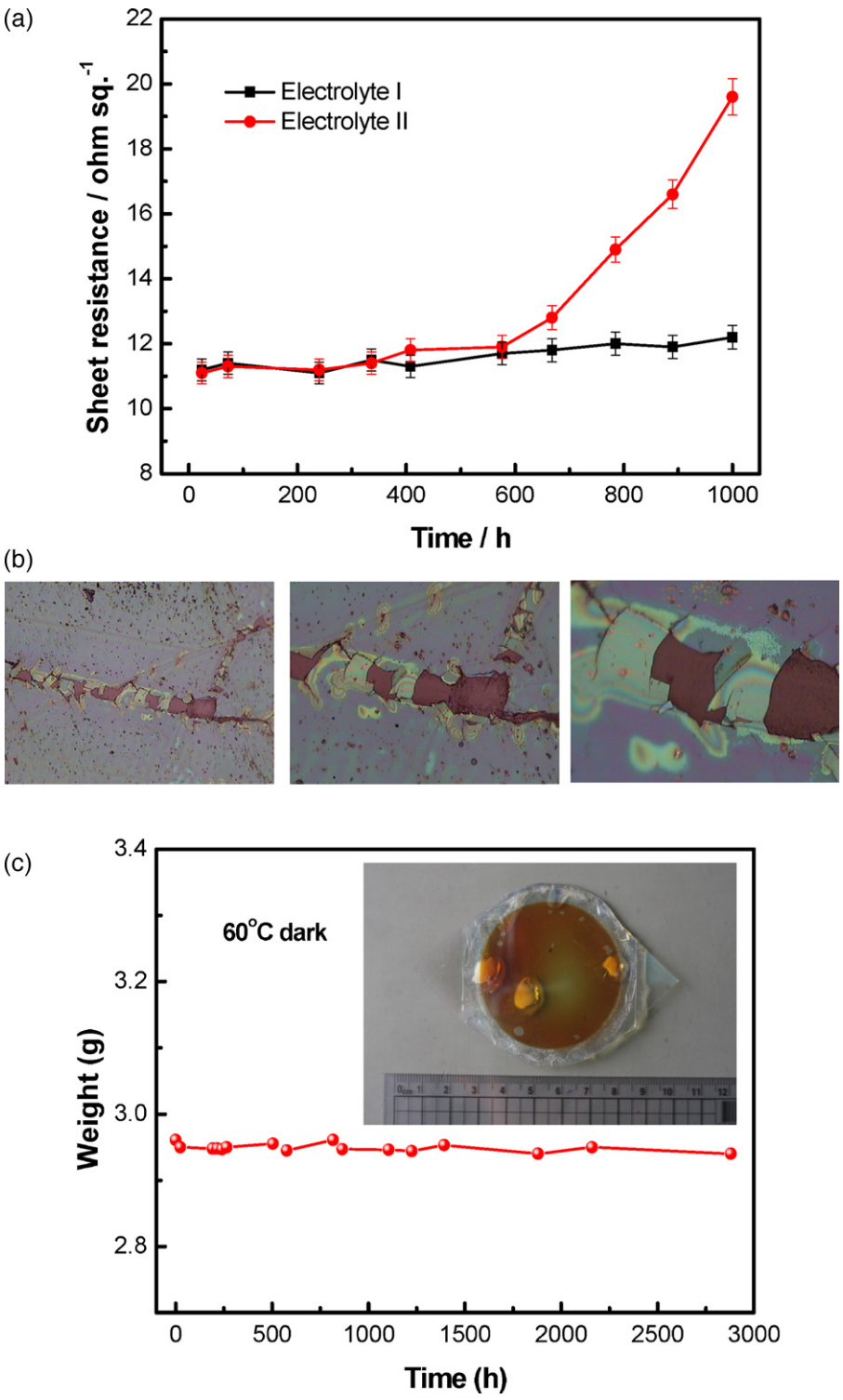

Fig. 4. (a) The relationship between the sheet resistance of ITO/PEN and the immersion time in electrolyte at 60 °C (electrolyte I: 0.5 M PMII and 0.05 M I_2 in MPN; electrolyte II: 0.5 M LiI and 0.05 M I_2 in MPN). (b) The OM images of ITO/PEN film after immersion in electrolyte II at 60 °C. (c) The sealing test cell and the weight loss of cell during thermal treatment at 60 °C in the dark.

the effective electron lifetime, τ_{eff}, increases with the light soaking time. It implies that the recombination of electrons with triiodide at the interface of TiO_2 NPs and the electrolyte has inhibited during the prolonged stability test resulting in a stable photocurrent output. Furthermore, the device with electrolyte I has a higher resistance of charge transfer at the Pt/electrolyte interface than that with electrolyte II as shown in Fig. 6. This means that the electrolyte containing TBAI had a lower triiodide reduction rate at the Pt/electrolyte interface that leads to the lower FF value as shown in Fig. 5.

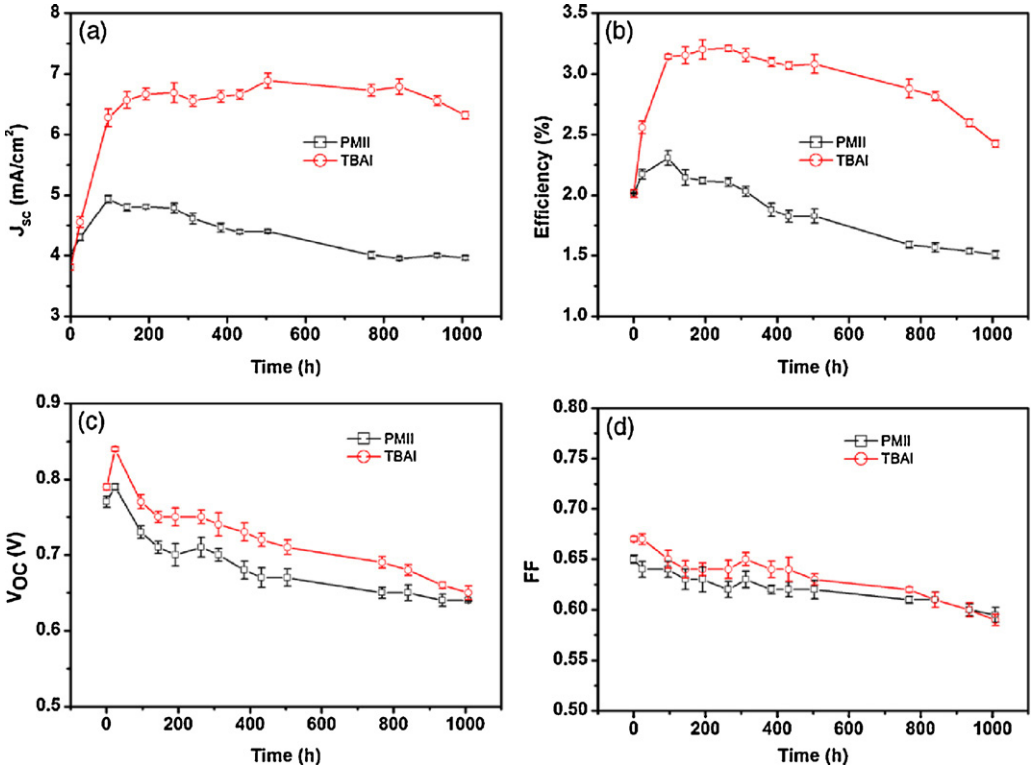

Fig. 5. Photovoltaic parameters for plastic DSSC with TBAI or PMII after visible light soaking (1 sun) at 60 °C. (a) Short circuit current density, J_{SC}; (b) Energy conversion efficiency, η; (c) Open circuit voltage, V_{OC} and (d) Fill factor, FF.

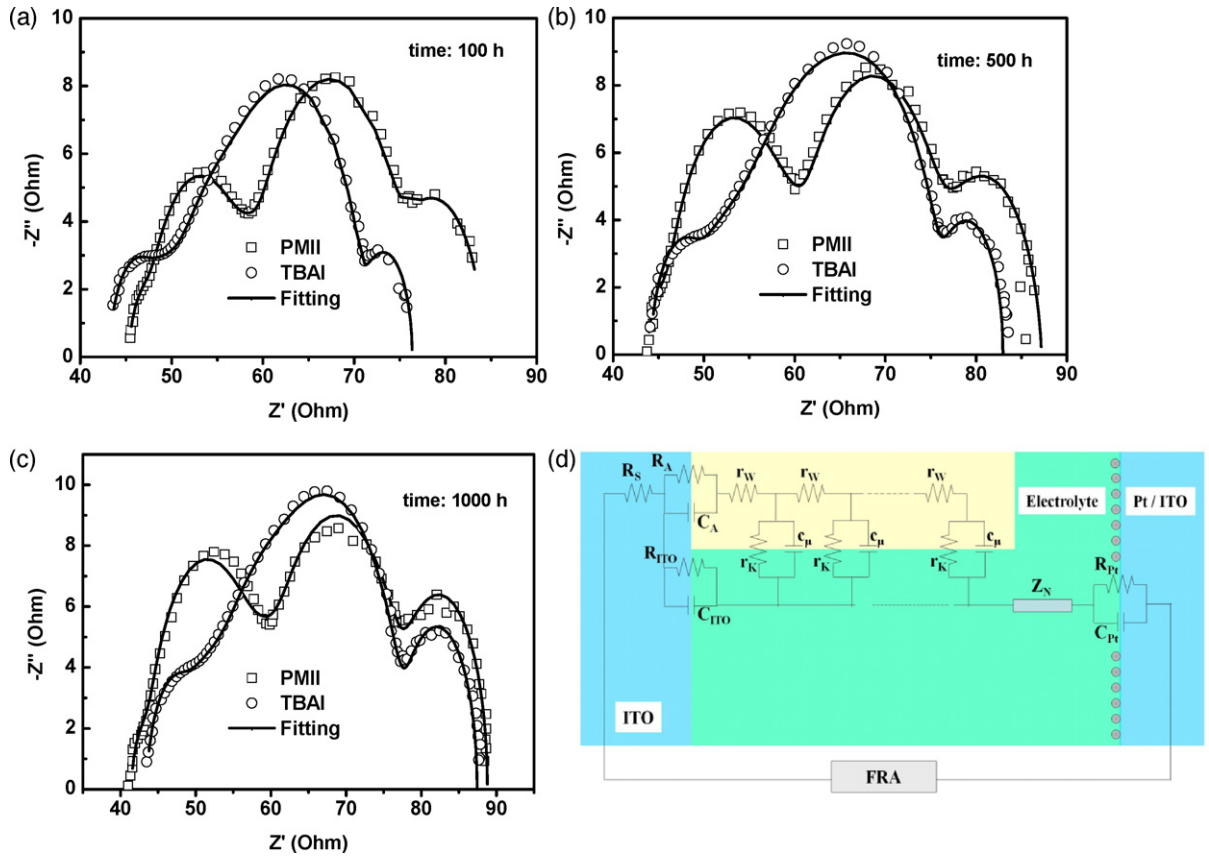

Fig. 6. EIS results of plastic DSSCs with different iodides after 1 sun light soaking for (a) 100, (b) 500 and (c) 1000 h. (d) The equivalent circuit model employed for fitting the EIS experimental results.

Table 2
Parameters determined from fitting EIS data of plastic DSSC with electrolytes containing TBAI and PMII, respectively.

Iodide	Light aging time (h)	R_w (Ω)	R_k (Ω)	R_k/R_w	τ_{eff} (ms)	D_{eff} (10^{-5} cm^2 s^{-1})	L_n (μm)
TBAI	100	12.9	13.5	1.05	36.8	1.02	6.2
	500	12.6	13.2	1.05	44.2	0.85	6.1
	1000	18.8	14.4	0.77	48.4	0.57	5.3
PMII	100	28.9	13.2	0.46	16.6	0.99	4.1
	500	37.4	14.3	0.38	15.3	0.90	3.7
	1000	41.4	14.4	0.35	14.5	0.86	3.5

4. Conclusions

We have investigated the durability of flexible devices with different cation iodides. Under prolonged one-sun light-irradiation and 60 °C-thermal stress aging, our plastic DSSC devices showed an initial improvement in performance of 96.9% followed by an extended steady-state period of more than 1000 h. The presence of TBAI in the electrolyte provides higher photocurrent and better durability. This improvement is a result of TBA^+ on the TiO_2 film surface, which sterically protects the voids in the dye-coated TiO_2 film in turn blocks undesirable interfacial charge recombination to suppress surface protonation.

Acknowledgements

We gratefully acknowledge the financial support of Industrial Technology Research Institute (ITRI) and the National Science Council of Taiwan (NSC-99-2112-M-006-017-MY3 and NSC-99-2221-E-009-095-MY3).

References

[1] M. Grätzel, Nature 414 (2001) 338–344.
[2] N.G. Park, K.M. Kim, M.G. Kang, K.S. Ryu, S.H. Chang, Y.J. Shin, Adv. Mater. 17 (2005) 2349–2353.
[3] D.S. Zhang, T. Yoshida, K. Furuta, H. Minoura, J. Photochem. Photobiol. A 164 (2004) 159–166.
[4] D.S. Zhang, T. Yoshida, H. Minoura, Adv. Mater. 15 (2003) 814–817.
[5] S. Uchida, M. Tomiha, H. Takizawa, M. Kawaraya, J. Photochem. Photobiol. A 164 (2004) 93–96.
[6] S. Uchida, M. Tomiha, N. Masaki, A. Miyazawa, H. Takizawa, Sol. Energy Mater. Sol. Cells 81 (2004) 135–139.
[7] T. Miyasaka, Y. Kijitori, J. Electrochem. Soc. 151 (2004) A1767–A1773.
[8] H. Lindström, A. Holmberg, E. Magnusson, L. Malmqvist, A. Hagfeldt, J. Photochem. Photobiol. A 145 (2001) 107–112.
[9] H. Lindström, A. Holmberg, E. Magnusson, S.E. Lindquist, L. Malmqvist, A. Hagfeldt, Nano Lett. 1 (2001) 97–100.
[10] G. Boschloo, H. Lindstrom, E. Magnusson, A. Holmberg, A. Hagfeldt, J. Photochem. Photobiol. A 148 (2002) 11–15.
[11] S.A. Haques, E. Palomares, H.M. Upadhyaya, L. Otley, R.J. Potter, A.B. Holmes, J.R. Durrant, Chem. Commun. (2003) 3008–3009.
[12] W.H. Chiu, K.M. Lee, W.F. Hsieh, J. Power Sources 198 (2011) 3683–3687.
[13] M. Ikegami, J. Suzuki, K. Teshima, M. Kawaraya, T. Miyasaka, Sol. Energy Mater. Sol. Cells 93 (2009) 836–839.
[14] P. Wang, S.M. Zakeeruddin, P. Comte, I. Exnar, M. Grätzel, J. Am. Chem. Soc. 125 (2003) 1166–1167.
[15] P. Wang, S.M. Zakeeruddin, I. Exnar, M. Grätzel, Chem. Commun. (2002) 2972–2973.
[16] N. Ikeda, K. Teshima, T. Miyasaka, Chem. Commun. (2006) 1733–1735.
[17] N. Ikeda, T. Miyasaka, Chem. Lett. 36 (2007) 466–467.
[18] O. Kohle, M. Grätzel, A.F. Meyer, T.B. Meyer, Adv. Mater. 9 (1997) 904–906.
[19] R. Kern, N. van der Burg, G. Chmiel, J. Ferber, G. Hasenhindl, A. Hinsch, R. Kinderman, J. Kroon, A. Meyer, T. Meyer, R. Niepmann, J. van Roosmalen, C. Schill, M. Sommeling, M. Späth, I. Uhlendorf, Opto-Electron. Rev. 8 (2000) 284–288.
[20] M. Sommeling, M. Späth, H.J.P. Smit, N.J. Bakker, J.M. Kroon, J. Photochem. Photobiol. A 164 (2004) 137–144.
[21] T. Toyoda, T. Sano, J. Nakajima, S. Doi, S. Fukumoto, A. Ito, T. Tohyama, M. Yoshida, T. Kanagawa, T. Motohiro, T. Shiga, K. Higuchi, H. Tanaka, Y. Takeda, T. Fukano, N. Katoh, A. Takeichi, K. Takechi, M. Shiozawa, J. Photochem. Photobiol. A 164 (2004) 203–207.
[22] D. Kuang, S. Ito, B. Wenger, C. Klein, J.E. Moser, R. Humphry-Baker, S.M. Zakeeruddin, M. Grätzel, J. Am. Chem. Soc. 128 (2006) 4146–4154.
[23] K.M. Lee, S.J. Wu, C.Y. Chen, C.G. Wu, M. Ikegami, K. Miyoshi, T. Miyasaka, K.C. Ho, J. Mater. Chem. 19 (2009) 5009–5015.
[24] L. Grinis, S. Dor, A. Ofir, A. Zaban, J. Photochem. Photobiol. A 198 (2008) 52–59.
[25] Z.S. Wang, H. Kawauchi, T. Kashima, H. Arakawa, Coord. Chem. Rev. 248 (2004) 1381–1389.
[26] T. Yamaguchi, N. Tobe, D. Matsumoto, T. Nagai, H. Arakawa, Sol. Energy Mater. Sol. Cells 94 (2010) 812–816.
[27] Z. Zhang, S. Ito, J.E. Moser, S.M. Zakeeruddin, M. Grätzel, ChemPhysChem 10 (2009) 1834–1838.
[28] C.Y. Chen, M. Wang, J.Y. Li, N. Pootrakulchote, L. Alibabaei, C.H. Ngoc-le, J.D. Decoppet, J.H. Tsai, C. Grätzel, C.G. Wu, S.M. Zakeeruddin, M. Grätzel, ACS Nano 3 (2009) 3103–3109.
[29] M. Wang, X. Li, H. Lin, P. Pechy, S.M. Zakeeruddin, M. Grätzel, Dalton Trans. (2009) 10015–10020.
[30] C.Y. Chen, N. Pootrakulchote, S.J. Wu, M. Wang, J.Y. Li, J.H. Tsai, C.G. Wu, S.M. Zakeeruddin, M. Grätzel, J. Phys. Chem. C 113 (2009) 20752–20757.
[31] M. Adachi, M. Sakamoto, J. Jiu, Y. Ogata, S. Isoda, J. Phys. Chem. B 110 (2006) 13872–13880.